

# Improved correction methods for field measurements of particulate light backscattering in turbid waters

David Doxaran,<sup>1,\*</sup> Edouard Leymarie,<sup>1</sup> Bouchra Nechad,<sup>2</sup> Ana Dogliotti,<sup>3</sup> Kevin Ruddick,<sup>2</sup> Pierre Gernez,<sup>4</sup> and Els Knaeps<sup>5</sup>

<sup>1</sup>Laboratoire d'Océanographie de Villefranche, CNRS-UPMC, France

<sup>2</sup>Royal Belgian Institute for Natural Sciences (RBINS), Operational Directorate Natural Environment, Brussels, Belgium

<sup>3</sup>Instituto de Astronomía y Física del Espacio (IAFE), CONICET/UBA, Argentina

<sup>4</sup>Université de Nantes, Mer Molécules Santé (EA 2160), France

<sup>5</sup>Flemish Institute for Technological Research (VITO), Belgium

\*doxaran@obs-vlfr.fr

**Abstract:** Monte Carlo simulations are used to compute the uncertainty associated to light backscattering measurements in turbid waters using the ECO-BB (WET Labs) and Hydroscat (HOBi Labs) scattering sensors. ECO-BB measurements provide an accurate estimate of the particulate volume scattering coefficient after correction for absorption along the short instrument pathlength. For Hydroscat measurements, because of a longer photon pathlength, both absorption and scattering effects must be corrected for. As the standard (sigma) correction potentially leads to large errors, an improved correction method is developed then validated using field inherent and apparent optical measurements carried out in turbid estuarine waters. Conclusions are also drawn to guide development of future short pathlength backscattering sensors for turbid waters.

©2016 Optical Society of America

**OCIS codes:** (010.0010) Atmospheric and oceanic optics; (010.4458) Oceanic scattering; (010.1350) Backscattering.

---

## References and links

1. H. R. Gordon, O. B. Brown, and M. M. Jacobs, "Computed relationships between the inherent and apparent optical properties of a flat homogeneous ocean," *Appl. Opt.* **14**(2), 417–427 (1975).
2. A. Morel and L. Prieur, "Analysis of variations in ocean color," *Limnol. Oceanogr.* **22**(4), 709–722 (1977).
3. G. Neukermans, H. Loisel, X. Mériaux, R. Astoreca, and D. McKee, "In situ variability of mass-specific beam attenuation and backscattering of marine particles with respect to particle size, density, and composition," *Limnol. Oceanogr.* **57**(1), 124–144 (2012).
4. A. Morel, "Diffusion de la lumière par les eaux de mer; résultats expérimentaux et approche théorique," AGARD Lecture Series, 3.1.1-3.1.76 (1973).
5. E. Boss, M. S. Twardowski, and S. Herring, "Shape of the particulate beam attenuation spectrum and its inversion to obtain the shape of the particulate size distribution," *Appl. Opt.* **40**(27), 4885–4893 (2001).
6. E. Boss, W. S. Pegau, W. D. Gardner, J. R. V. Zaneveld, A. H. Barnard, M. S. Twardowski, G. C. Chang and T. D. Dicke, "Spectral particulate and particle size distribution in the bottom boundary layer of a continental shelf," *J. Geophys. Res.* **106**, 9509–9516 (2001).
7. W. H. Slade and E. Boss, "Spectral attenuation and backscattering as indicators of average particle size," *Appl. Opt.* **54**(24), 7264–7277 (2015).
8. E. Boss and W. S. Pegau, "Relationship of light scattering at an angle in the backward direction to the backscattering coefficient," *Appl. Opt.* **40**(30), 5503–5507 (2001).
9. R. A. Maffione and D. R. Dana, "Instruments and methods for measuring the backward-scattering coefficient of ocean waters," *Appl. Opt.* **36**(24), 6057–6067 (1997).
10. D. R. Dana and R. A. Maffione, "Determining the Backward Scattering Coefficient with Fixed-Angle Backscattering Sensors? Revisited," in *Ocean Optics XVI Conference* (2002).
11. WET Labs ECO BB User's Guide (BB), Revision AC, 11 Sept. 2007.
12. E. Leymarie, D. Doxaran, and M. Babin, "Uncertainties associated to measurements of inherent optical properties in natural waters," *Appl. Opt.* **49**(28), 5415–5436 (2010).
13. C. D. Mobley, *Light and Water* (Academic, 1994).

14. M. Sullivan, M. S. Twardowski, J. R. V. Zaneveld, and C. C. Moore, "Chapter 6: Measuring optical backscattering in water," in *Light Scattering Reviews 7: Radiative Transfer and Optical Properties of Atmosphere and Underlying Surface*, A. A. Kokhanovsky, ed. (S Praxis Books, 2013).
15. AC-9 User's Guide (AC-9), WET Labs Inc., Revision S, June 2008.
16. Backscattering Sensor Calibration Manual HydroScat-2, HydroScat-4, HydroScat-6, a-Beta and c-Beta. Hydro-Optics, Biology, & Instrumentation Laboratories, Inc., Revision N, Oct. 2008.
17. HydroSoft 2.9 Software for HOBI Labs Optical Oceanographic Instruments User's Manual. Hydro-Optics, Biology & Instrumentation Laboratories, Revision H, Feb. 2012.
18. M. S. Twardowski, E. Boss, J. B. Macdonald, W. S. Pegau, A. H. Barnard, and J. R. V. Zaneveld, "A model for estimating bulk refractive index from the optical backscattering ratio and the implications for understanding particle composition in case I and case II waters," *J. Geophys. Res.* **106**(C7), 14129–14142 (2001).
19. M. Chami, E. Marken, J. J. Stamnes, G. Khomenko, and G. Korotaev, "Variability of the relationship between the particulate backscattering coefficient and the volume scattering function measured at fixed angles," *J. Geophys. Res.* **111**(C5), C05013 (2006).
20. J. M. Sullivan and M. S. Twardowski, "Angular shape of the oceanic particulate volume scattering function in the backward direction," *Appl. Opt.* **48**(35), 6811–6819 (2009).
21. M. S. Twardowski and W. E. T. Labs, Inc., 70 Dean Knauss Dr., Narragansett, RI 02882, USA (personal communication, 2014).
22. D. Dana, Hobi Instrument Services, 12819 SE 38th St. #434, Bellevue, WA 98006, USA (personal communication, 2013).
23. Backscattering sensor calibration manual HydroScat-2, HydroScat-4, HydroScat-6, a-Beta and c-Beta, Revision N. Hydro-Optics, Biology and Instrumentation Laboratories, Inc, Oct. 2008.
24. SeaSWIR research project, <http://www.seaswir.vgt.vito.be/>
25. R. M. Pope and E. S. Fry, "Absorption spectrum (380–700 nm) of pure water. II. Integrating cavity measurements," *Appl. Opt.* **36**(33), 8710–8723 (1997).
26. L. Kou, D. Labrie, and P. Chylek, "Refractive indices of water and ice in the 0.65- to 2.5- $\mu$ m spectral range," *Appl. Opt.* **32**(19), 3531–3540 (1993).
27. C. D. Mobley, L. K. Sundman, and E. Boss, "Phase function effects on oceanic light fields," *Appl. Opt.* **41**(6), 1035–1050 (2002).
28. A. I. Dogliotti, K. G. Ruddick, B. Nechad, D. Doxaran, and E. Knaeps, "A single algorithm to retrieve turbidity from remotely sensed data in all coastal and estuarine waters," *Remote Sens. Environ.* **156**, 157–168 (2015).
29. P. Gernez, L. Barillé, A. Lerouxel, C. Mazeran, A. Lucas, and D. Doxaran, "Remote sensing of suspended particulate matter in turbid oyster-farming ecosystem," *J. Geophys. Res. Oceans* **119**(10), 7277–7294 (2014).
30. J. R. V. Zaneveld, J. C. Kitchen, and C. C. Moore, "Scattering error correction of reflecting tube absorption meter," *Proc. SPIE* **2258**, 44–55 (1994).
31. D. Doxaran, M. Babin, and E. Leymarie, "Near-infrared light scattering by particles in coastal waters," *Opt. Express* **15**(20), 12834–12849 (2007).
32. D. Doxaran, K. Ruddick, D. McKee, B. Gentili, D. Tailliez, M. Chami, and M. Babin, "Spectral variations of light scattering by marine particles in coastal waters, from the visible to the near infrared," *Limnol. Oceanogr.* **54**(4), 1257–1271 (2009).
33. R. Röttgers and S. Gehrke, "Measurement of light absorption by aquatic particles: improvement of the quantitative filter technique by use of an integrating sphere approach," *Appl. Opt.* **51**(9), 1336–1351 (2012).
34. R. Röttgers, C. Dupouy, B. B. Taylor, A. Bracher, and S. B. Woźniak, "Mass-specific light absorption coefficients of natural aquatic particles in the near-infrared spectral region," *Limnol. Oceanogr.* **59**(5), 1449–1460 (2014).
35. J. L. Mueller, C. Davis, R. A. Arnone, R. Frouin, K. Carder, Z. P. Lee, R. G. Steward, S. Hooker, C. D. Mobley, and S. McLean, "Above-water radiance and remote sensing reflectance measurements and analysis protocols," in *Ocean Optics Protocols for Satellite Ocean Color Sensor Validation. Revision 2*, G. S. Fargion and J. L. Mueller, ed. (National Aeronautical and Space Administration, 2000).
36. C. D. Mobley, "Estimation of the remote-sensing reflectance from above-surface measurements," *Appl. Opt.* **38**(36), 7442–7455 (1999).
37. K. G. Ruddick, V. De Cauwer, Y. J. Park, and G. Moore, "Seaborne measurements of near infrared water-leaving reflectance: The similarity spectrum for turbid waters," *Limnol. Oceanogr.* **51**(2), 1167–1179 (2006).
38. A. Morel, "Optical properties of pure water and pure seawater," in *Optical Aspects of Oceanography*, N. G. Jerlov & E. Steeman Nielsen, ed. (Academic, 1974).
39. D. Segelstein, "The complex refractive index of water," M.S. Thesis, Missouri U., Kansas City (1981).
40. A. L. Whitmire, E. Boss, T. J. Cowles, and W. S. Pegau, "Spectral variability of the particulate backscattering ratio," *Opt. Express* **15**(11), 7019–7031 (2007).
41. W. A. Snyder, R. A. Arnone, C. O. Davis, W. Goode, R. W. Gould, S. Ladner, G. Lamela, W. J. Rhea, R. Stavn, M. Sydor, and A. Weidemann, "Optical scattering and backscattering by organic and inorganic particulates in U.S. coastal waters," *Appl. Opt.* **47**(5), 666–677 (2008).
42. D. McKee, M. Chami, I. Brown, V. S. Calzado, D. Doxaran, and A. Cunningham, "Role of measurement uncertainties in observed variability in the spectral backscattering ratio: a case study in mineral-rich coastal waters," *Appl. Opt.* **48**(24), 4663–4675 (2009).

## 1. Introduction

Mapping of Suspended Particulate Matter (SPM) from space provides information for a variety of applications including dynamics of suspended particles (phytoplankton blooms, river plumes, coastal erosion) and water quality monitoring. Ocean colour data processing generally retrieves explicitly or implicitly the absorption and backscattering coefficients,  $a$  and  $b_b$  in  $\text{m}^{-1}$ , because of the strong relationship between reflectance and these two inherent optical properties (IOPs) [1,2]. By subtracting the known contribution of pure seawater ( $b_{pw}$ ) it is then straightforward to retrieve the particulate backscattering coefficient ( $b_{bp}$ ) which contains information on the concentration and composition (refractive index) of suspended particles [3]. Information on the size distribution of hydrosols can also be obtained from the spectral variations of the  $b_{bp}$  coefficient [4–6] (at least information reflective of average particle size [7]). Accurate spectral  $b_{bp}$  measurements are therefore crucial in natural waters for the interpretation of the water reflectance signal and retrieval of key biogeochemical parameters required for the monitoring of phytoplankton blooms, water quality, sediment transport and river discharge in the coastal ocean.

Several light backscattering sensors have been designed and widely used by the ocean colour community, such as the ECO-BB (WET Labs) and Hydrosat (HOBi Labs) devices. These sensors include a light source (LED at different wavelengths covering the visible and near-infrared (NIR) spectral domains) and detectors with a narrow field-of-view (FOV) to collect the light backscattered at a fixed angle (varying from 120 to 140°) and provide a measurement of the volume scattering function (VSF) at this angle:  $\beta$ , in  $\text{m}^{-1} \text{sr}^{-1}$ . The particulate VSF,  $\beta_p$ , is then obtained by removing from the measured signal the pure seawater contribution. Backscattering angles around 120 and 140° were chosen in order to minimize the uncertainty when extrapolating  $\beta_p$  to  $b_{bp}$  [8–10]. These two devices were originally designed for open ocean waters with low scattering and problems are often encountered when measuring in turbid coastal waters. The main problems are (i) the correction of the measured signal for absorption and scattering losses, (ii) the interpretation of the signal measured in multi-scattering regimes and (iii) the saturation of sensors designed to sample clear ocean waters. The ECO-BB sensor notably has a fixed high sensitivity which usually leads to a saturated signal in highly scattering waters. The Hydrosat sensor is better adapted in the case of turbid coastal waters as it has five adaptive gains which take into account the amount of backscattered light and allow adapting the sensor sensitivity accordingly. Because of its small dimensions and a resulting short photon pathlength, ECO-BB measurements are supposed to be corrected only for photon losses due to light absorption (on top of pure water absorption) [11]. Due to the larger dimensions of the Hydrosat-4 and 6 sensors and so the longer instrument pathlength, losses due to absorption and scattering are accounted for when applying the ‘sigma’ correction [10]. Without justification/demonstration to our knowledge, this correction assumes that photon losses along their pathlength can be accurately estimated as the absorption coefficient plus 40% (0.4) of the scattering coefficient (where both coefficients exclude the pure water contribution). This assumption has probably limited implications in the case of predominantly light absorbing waters (e.g., open ocean waters during non-bloom conditions) but may result in great errors when dealing with highly scattering mineral-rich coastal waters.

The first objective of the present study is to assess how accurately the particulate VSF (at specific angles) can be measured in turbid coastal waters using ECO-BB and Hydrosat sensors and determine the validity of such measurements in the case of a multi-scattering regime. A second objective is to test the performance of the measurement corrections recommended by the manufacturers [10,11] in turbid waters notably in the case of increasing loads of predominantly mineral-rich suspended particles, i.e., for increasing particulate (back)scattering coefficients. The third objective is to improve, when necessary, the recommended correction methods and validate them based on field measurements.

## 2. Data and methods

In order to meet the proposed objectives, a three-step methodology is used. First, taking into account the geometrical configurations of the ECO-BB and Hydrosat sensors, the SimulO Monte Carlo code [12] is used to test and parameterize the optimal correction method for accurate retrieval of the  $\beta_p$  signal in a wide range of natural waters. Second, in the case of Hydrosat measurements, the standard sigma and a new correction methods are both applied to two field data sets of IOPs representative of turbid coastal waters. Results are then used as inputs in the Hydrolight radiative transfer code [13] to compute the remote sensing reflectance ( $R_{rs}$ ) signal. The validity of the results obtained is finally assessed comparing Hydrolight outputs to  $R_{rs}$  spectral values independently measured in the field (optical closure). Results are finally used to define the specifications of the ideal scattering sensor in the case of turbid coastal waters.

### 2.1 Scattering sensors and data corrections

The ECO-BB sensor measures the  $\beta$  signal around the backscattering angle of  $124^\circ$  (and not  $117^\circ$  as initially stated [14]). Because of the small dimensions of the sensor (i.e., light source to detector distance), the instrument pathlength is quite short ( $< 0.05$  m, see Table 1). Therefore WET Labs assumes that loss of photons due to scattering is negligible and only loss by absorption should be accounted for and corrected according to:

$$\beta_{cor}(124^\circ, a_{nw} = 0) = \beta_{meas}(124^\circ, a_{nw}) \times \exp(0.0391 \times a_{nw}), \quad (1)$$

where  $a_{nw}$ , in  $m^{-1}$ , where ‘nw’ stands for non-water, is the absorption coefficient after subtraction of the pure water contribution (i.e., light absorption by coloured suspended particles and dissolved organic matter). This  $a_{nw}$  coefficient can be measured with a WET Labs AC device (since calibration of such sensors is made with respect to pure water [15]).  $\beta_{meas}$  and  $\beta_{cor}$  are respectively the measured and corrected  $\beta$  values.

Hydrosat sensors have larger dimensions and consequently a significantly longer instrument pathlength compared to the ECO-BB sensor (Table 1). Also HOBI Labs recommends correcting the measured  $\beta$  signal for loss of photons due to both absorption and scattering. Similar to Eq. (1) for the ECO-BB, the sigma correction method recommended by HOBI Labs is expressed as [16,17]:

$$\beta_{cor} = \exp(k_{exp} \times K_{bb}) \times \beta_{meas}, \quad (2)$$

but here  $K_{bb}$  is the attenuation of photons travelling from the sensor light source to the detector, i.e., attenuation due to both light absorption and scattering on top of pure water. The  $k_{exp}$  coefficient is a distance (instrument pathlength) which is slightly wavelength-dependent; it includes light attenuation due to pure water in which each sensor is calibrated, and is specific to each instrument and wavelength (it is provided in the calibration file).

The  $K_{bb}$  attenuation coefficient is expressed as:

$$K_{bb} = a_{nw} + K_{scat} \times b_{nw}, \quad (3)$$

with  $K_{scat}$ , the percentage of light scattering resulting in a loss of photons along the instrument pathlength, set to a constant value of 0.4 (i.e., 40%) by the manufacturer [9]. Note that this constant value of 0.4 was set somehow arbitrarily and was never demonstrated to our knowledge.

It is logical to expect that the loss of photons between the sensor light source and detector is equal to the absorption coefficient of the medium plus a certain percentage of the scattering coefficient. However there is neither reason nor demonstration showing that a fixed value of 40% of the photons scattered along their pathlength will be lost and not detected. Moreover, one may expect the percentage of scattered light that is lost for detection to vary significantly depending on the size distribution and chemical composition of suspended particles, which

both present wide variations in natural waters. These variations are well known to induce significant changes in the particulate backscattering ratio [18].

Note that our study is only focused on the uncertainty associated with  $\beta$  measured in turbid natural waters. Additional uncertainties are associated to the estimation of  $b_{bp}$  which is obtained after subtracting from  $\beta_{cor}$  the known contribution of pure water ( $\beta_w$ ) as:

$$b_{bp} = 2\pi \times \chi \times (\beta_{cor} - \beta_w). \quad (4)$$

The  $\chi$  factor is usually set to constant values of 1.1 and 1.08, respectively, for the ECO-BB and Hydroscat sensors [6, 9], even if it has been shown that  $\chi$  is actually not constant [19]. The variations of the particulate VSF in the backward direction have been proved to be quite limited based on numerous field measurements [20] but should not be neglected in the case of unusual particle size distributions and/or particle refractive index. This further step introduces additional uncertainties on the final parameter,  $b_{bp}$ , but this is outside the scope of the present study.

**Table 1. Specifications of the ECO-BB (WET Labs), Hydroscat-4 and Hydroscat-6 (HOBi Labs) scattering sensors.**

Sensor specifications	ECO-BB	Hydroscat-4	Hydroscat-6
Scattering angle (°)	~124	141	141
LED angular divergence (°)	15	4	4
Detector FOV (°, half angle)	15	3	3
Distance between source and detector axes (m)	0.008	0.058	0.070
Instrument pathlength (m)	0.0391* 0.01635**	0.1058	0.1502

\*defined in the the User's Guide, \*\*found in this study

## 2.2 Monte Carlo simulations

SimulO is a Monte Carlo code developed to easily simulate many types of optical devices, especially in the field of marine optics [12]. It is a natural three-dimensional (3D) forward Monte Carlo code, which implies that each photon is followed, one at a time, from the source to the point where it is absorbed. Using this code, complex optical devices can be simulated by positioning and sizing any number of elementary virtual objects. It allows reproducing IOP sensors taking into account their specifications in terms of geometry, dimensions, light source and detectors, imposing true IOPs typical of natural waters. Computations reproduce the IOPs that would actually be measured by the sensor after correcting for photon losses. The difference between the true and corrected IOPs is representative of the measurement uncertainty associated to the virtual sensor.

The exact designs of the ECO-BB, Hydroscat-4 (HS-4) and Hydroscat-6 (HS-6) sensors were respectively provided by WET Labs [21] and HOBi Labs [22] (Table 1). They were reproduced with SimulO using elementary virtual objects. The ECO-BB sensor (Fig. 1(a)) was modelled using two cylinders (diameters of 5 mm for the LED and 10 mm for the detector) with a relative refractive index of 1.56 and tilted at 26° from the horizontal axis allowing a theoretical measured scattering angle of 120° in water. A source point was positioned in the centre of the LED cylinder. LED angular divergence and detector FOV are determined only by the geometrical constraints and the light emission (sensitivity) is isotropic within this configuration. The Hydroscat sensors were modelled in 3D as a piece of transparent material (relative refractive index of 1.49) with two air holes ( $n = 1$ ) tilted at 45° (Fig. 1(b)) and two cylindrical windows. Within the two holes were set two cylinders: one for the LED (diameters: 5 mm for the HS-4 and 10 mm for the HS-6) and one for the detector

(diameter: 20 mm). The distances between the two windows central axes are respectively 58 mm and 70 mm for the HS-4 and HS-6. The LED angular divergence is  $4^\circ$  (half angle) and the detector FOV is  $3^\circ$  (half angle) which both determine the resulting trajectory of photons. Light emission and counting within these angles are isotropic. The virtual HydrosCat sensors were validated by reproducing sensitivity tests provided by the manufacturer, e.g., the  $\mu$ -calibration experiment performed by HOBI Labs (Fig. 1(c)). In such in-water experiments, the instrument is facing a diffuse white plaque which is moved away from the instrument within its sensitive range [23].

The IOPs (total absorption and attenuation coefficients, respectively  $a$  and  $c$  in  $\text{m}^{-1}$ ), various particulate volume scattering functions ( $\beta_p$ ) and backscattering ratios ( $b_{bp}/b_p$ ) typical of clear to extremely turbid (i.e., highly-absorbing and/or highly-scattering) waters were considered as SimulO inputs. These IOP values were set in order to be representative of their natural variations from 400 to 850 nm, i.e., from the visible to the NIR spectral domains. An additional wavelength in the shortwave-infrared (SWIR) region was also considered: 1020 nm. The objective here was notably to obtain results useful for the processing of data recorded by one HS-4 sensor specially designed to sample highly turbid waters [24] and equipped with the following four wavelengths: 550, 700, 850 and 1020 nm. The variations of the total absorption coefficient were therefore mainly driven by those of pure water which increases from  $0.0565 \text{ m}^{-1}$  at 550 nm [25] up to  $29.3 \text{ m}^{-1}$  at 1020 nm [26]. On top of pure water, the contributions of the other coloured water constituents, (phytoplankton, non-algal particles (NAP) and coloured dissolved organic matter (CDOM)) to light absorption and scattering in natural waters were also considered. To simplify the generation of the data set and make it independent of wavelength, we considered a regular grid of total absorption and scattering coefficients varying from 0 to  $10 \text{ m}^{-1}$  (absorption) and from 0 to  $50 \text{ m}^{-1}$  (scattering). All the possible combinations between the values of these coefficients were considered, in order to cover the wide range of optical properties encountered in natural waters. Additional computations were made varying the scattering coefficient and with a fixed absorption coefficient of  $30 \text{ m}^{-1}$  to simulate the SWIR wavelength of 1020 nm. Finally several particulate VSFs were considered: Fournier-Forand (FF) phase functions with spectrally-flat particulate backscattering ratios of 0.5, 1, 2, 4 and 5% [27], totaling more than 300 simulated combinations.

The results of the simulations are the numbers of photons detected by the sensor, i.e., entering the detector FOV normalized to the number of emitted photons. These raw results were then ‘calibrated’, i.e., converted into the physical unit of  $\beta$  ( $\text{m}^{-1} \text{ sr}^{-1}$ ). In order to do this, the average number of photons detected in simulations corresponding to the less turbid waters ( $c \leq 1 \text{ m}^{-1}$ ) was divided by the true (imposed)  $\beta_{\text{True}}$  value to get the calibration coefficient of the virtual sensor. It means that our simulated sensor was virtually calibrated in the spectral domain where the total absorption and scattering coefficients were minimum, i.e., in the green spectral region in our case for the visible and NIR spectral domains. Our virtual HS-4 sensor was also specifically calibrated in the SWIR for absorption and scattering coefficients of respectively  $30 \text{ m}^{-1}$  (close to the absorption coefficient of pure water at 1020 nm) and  $0.1 \text{ m}^{-1}$ . From our computations using SimulO, a value of 0.1058 was obtained for  $k_{\text{exp}}$  from the HS-4 plaque experiment (Fig. 1) (we found 0.1502 for the HS-6), which is quite close to typical calibration coefficients provided by HOBI Labs (from 0.09 to 0.12 for our HS-4 sensor).

The validity of the corrections applied to ECO-BB and HydrosCat data (Eqs. (1)–(3)) in a wide range of natural waters including highly scattering waters are here tested based on our SimulO computations. The method simply consists in relating the true ( $\beta_{\text{True}}$ ) and measured ( $\beta_{\text{meas}}$ ) signals knowing the values of  $a_{\text{nw}}$ ,  $b_p$  and  $b_{bp}$  which can be measured or derived from field IOP measurements. If not satisfactory, results of computations are used to develop an improved version of the recommended correction methods.

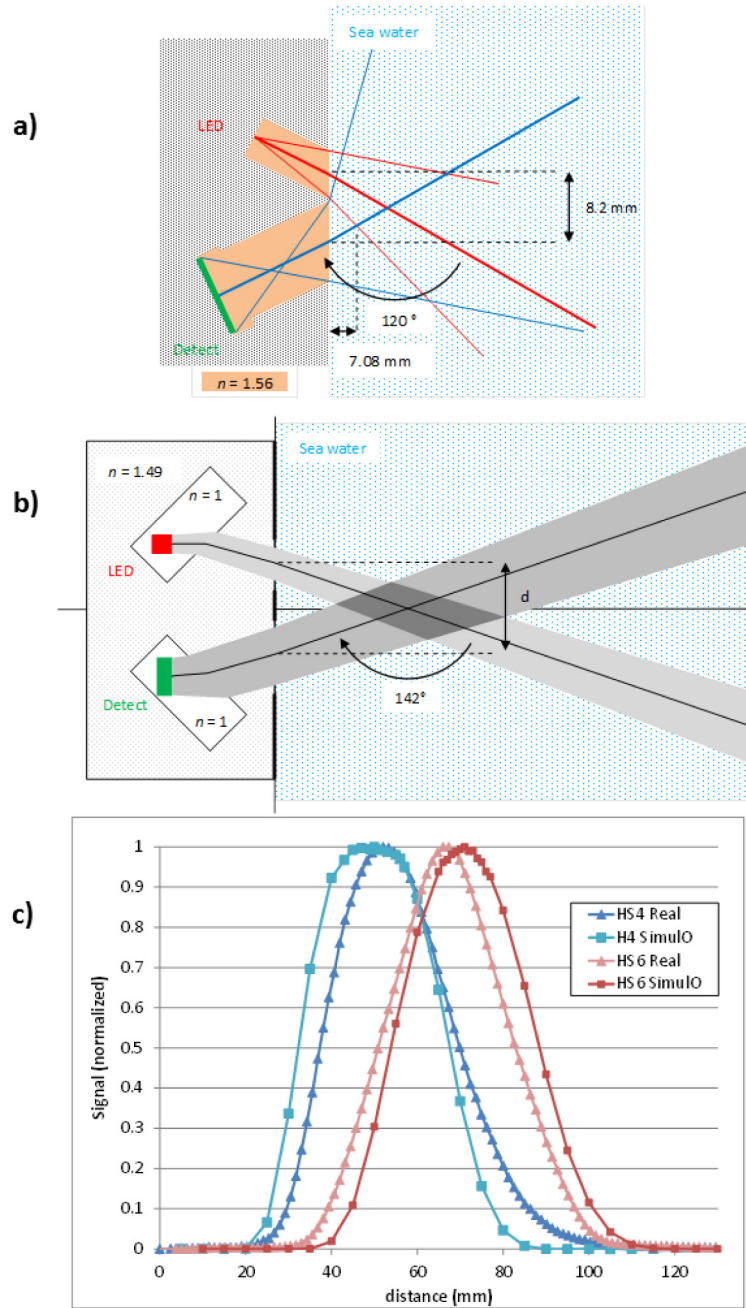


Fig. 1. (a) Schematic view of the ECO-BB sensor as reproduced using SimulO. (b) Schematic view of the Hydroscat sensors as reproduced using SimulO. Geometry of the virtual objects including the light sources (LED) and detectors and different media characterized by their respective relative refractive index ( $n$ ); the distances ( $d$ ) between source and detector axes are 0.058 and 0.070 m, respectively, for the HS-4 and HS-6 sensors. (c) Measured (laboratory experiment) and modelled (SimulO) response curves of Hydroscat sensors.

### 2.3 Field measurements

Field measurements of IOPs,  $Rrs$  and concentrations of suspended particulate matter (SPM in  $\text{g m}^{-3}$ ) were carried out in two shallow estuarine environments characterized by high concentrations of suspended sediments: the Río de la Plata (Argentina) and Bay of Bourgneuf (France). The Río de la Plata turbid waters were sampled on 19, 21, 22 and 23 November 2012 in Buenos Aires (Argentina), from the extremity of a 500 m long pier known as the Fisherman's Club (location:  $34^{\circ}55.8^{\circ}\text{S}$  and  $50^{\circ}40.2^{\circ}\text{W}$ ), for a total of 40 stations [28]. The Bay of Bourgneuf waters were sampled on 8 and 11 April 2013 onboard the Tzigane II vessel, as close as possible to intertidal mudflats, on a total of 14 stations [29].

The exact same measurement protocols were followed in the two study areas. A bucket was used to collect water samples just below the air-water interface during optical measurements. The water was filtered in triplicate through pre-weighed Whatman GF/F glass-fiber filters. Filters were then frozen until being dried (24 h at  $60^{\circ}\text{C}$ ) and weighed again to determine the dry weight of suspended particles in the volume of water filtered. The resulting SPM concentrations considering both sites were observed to vary from 30 to  $159 \text{ g m}^{-3}$  (mean value of  $68 \text{ g m}^{-3}$ ) and the measurement uncertainty was assumed to be the standard deviation between triplicates (13%, on average).

The IOPs were measured continuously by deploying sensors just below the water surface (0.5 meter depth), in a frame which included: (i) one conductivity, temperature and pressure sensor (SBE 49 Fastcat, Sea-Bird Electronics Inc.); (ii) one multi-spectral photometer (AC-9, WET Labs Inc.) equipped with 10 cm pathlength tubes measuring  $a_{nw}$  and  $c_{nw}$  at the following wavelengths: 440, 555, 630, 715, 730, 750, 767, 820 and 870 nm and (iii) one backscattering sensor (HS-4, HOBI Labs Inc.) measuring at the following wavelengths: 550, 700, 850 and 1020 nm.

Light absorption and attenuation measurements recorded by the AC-9 (previously calibrated in the lab using pure water) were first corrected for temperature and salinity effects [15]. The resulting absorption values were then corrected for residual scattering effects using the proportional method [30] and 870 nm as the reference wavelength where light absorption by coloured water constituents was assumed to be negligible [31,32]. Based on recent results, light absorption by non-algal particles may actually be significant in this spectral region [33,34] but low (compared to light absorption in the visible spectral domain) and difficult to quantify without ancillary data (e.g., measurements with a point-source integrating-cavity absorption meter). Particulate light scattering coefficients ( $b_p$ , in  $\text{m}^{-1}$ ) were obtained by subtracting the resulting absorption coefficients from the attenuation coefficients. A wide range of IOPs was covered during these field experiments (Fig. 2).



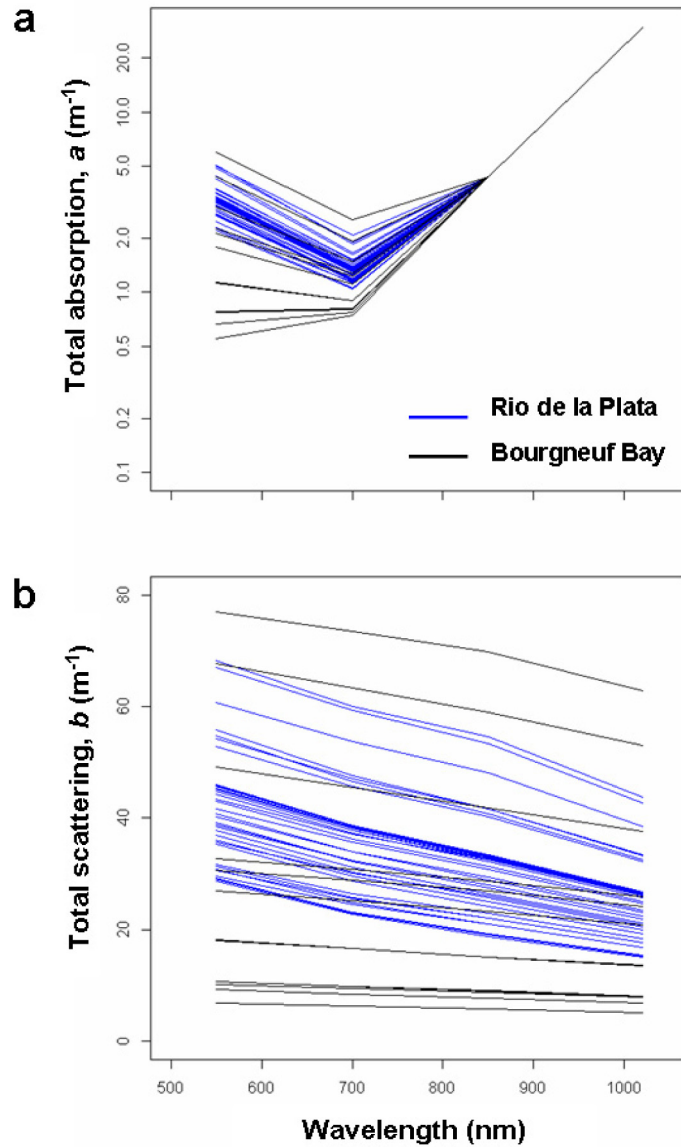


Fig. 2. Total absorption (a) and scattering (b) coefficients measured in the Río de la Plata (blue) and Bay of Bourgneuf (black) at 550, 700 and 850 nm and extrapolated at 1020 nm

Above-water reflectance measurements were made using a 3-sensor Trios system and one ASD Fieldspec FR spectrometer. Remote sensing reflectance was calculated from simultaneous above-water measurements of downwelling irradiance,  $E_d^{0+}$ , total upwelling radiance (i.e., from the water and from the air-sea interface) at a zenith angle of  $40^\circ$ ,  $L_u^{0+}$ , and sky radiance,  $L_{sky}^{0+}$ , in the direction of the region of sky that reflects into the seaviewing sensor, as [35, 36]:

$$R_{rs} = \frac{L_u^{0+} - \rho_{sky} \times L_{sky}^{0+}}{E_d^{0+}}, \quad (5)$$

where  $\rho_{sky}$  is the air-water interface reflection coefficient for radiance equal to the Fresnel reflection coefficient in the case of a flat sea surface. The solar azimuth angle was systematically set to  $90^\circ$ . In the case of the Trios system, the irradiance sensor was oriented vertically to zenith while  $L_{sky}^{0+}$ ,  $L_u^{0+}$  and  $E_d^{0+}$  measurements were recorded simultaneously from 350 to 900 nm during about 5 minutes of apparently stable sky conditions with a spectral resolution of 2.5 nm. In the case of ASD having only one radiometer, the sensor was pointed successively towards (i) the water with a  $40^\circ$  zenith angle, (ii) the region of sky that reflects into the seaviewing sensor at  $40^\circ$  nadir angle and (iii) the nadir facing a white (approx. 100% reflectance) Spectralon panel to measure, respectively,  $L_u^{0+}$ ,  $L_{sky}^{0+}$  and  $L_d^{0+}$  from 350 to 2500 nm. The downwelling radiance,  $L_d^{0+}$ , was multiplied by  $\pi$  sr and by the exact reflectance of the calibrated Spectralon panel to retrieve the  $E_d^{0+}$  signal. The spectral resolution of the ASD sensor was 1.4 nm (350-1000 nm) and 2 nm (1000-2500 nm).

As in Ruddick et al. (2006) for cloudy sky conditions [37],  $\rho_{sky}$  was set to the constant value of 0.0256, i.e., we did not use a wind speed formulation for  $\rho_{sky}$  as measurements were made in fetch-limited estuaries. As there is no robust model for  $\rho_{sky}$  in the case of partially cloudy skies, the corresponding radiometric measurements were removed from the data set. For ASD measurements, the resulting  $Rrs$  signal at 1200 nm was subtracted from the whole spectrum to correct for any residual sky glint correction. A careful quality check [37] was applied to the remaining data which were then averaged over the 5 minutes measurement intervals to obtain the mean values of  $Rrs$  at each station and the corresponding standard deviations. Only  $Rrs$  measurements at 550, 700, 850 and 1020 nm (only ASD) were considered further in this study.

#### 2.4 Hydrolight computations—Optical closure

The pure water contribution [25, 26, 38, 39] was added to the IOPs measured with the AC-9 to obtain the total light and scattering coefficients of the sampled waters at the HS-4 wavelengths (Fig. 2). At 850 and 1020 nm, light absorption by coloured water constituents was assumed to be negligible so that total absorption is only the contribution of pure water. A power-law function was fitted to the particulate scattering coefficient measured at 550, 715 and 870 nm to determine  $b_p$  then the total scattering  $b$  at 1020 nm.

For each station, the exact time, location (latitude and longitude) and IOPs (i.e., total absorption and scattering coefficients, particulate backscattering ratio) were used as inputs in the Hydrolight radiative transfer code version 5.1 [13] to compute the  $Rrs$  signal. A semi-empirical sky radiance distribution (model based on RADTRAN) was imposed specifying the sky cloud cover (in %). As outputs, the  $Rrs$  signal was computed as at the exact measurement zenith and azimuth angles and at 550, 700, 850 and 1020 nm for direct comparison with  $Rrs$  field measurements (optical closure).

### 3. Results

#### 3.1 Bio-optical properties (field data sets)

Spectral variations of the total absorption coefficient mainly result from the very high absorption by pure water in the NIR and SWIR spectral regions (Fig. 2(a)). A very significant contribution to light absorption by coloured dissolved matter and non-algal particles is observed at 550 nm where total absorption varies from 0.5 to more than  $5 \text{ m}^{-1}$  in the moderately to highly turbid waters of the Bay of Bourgneuf and Río de la Plata. Smoother spectral variations are associated with the total scattering coefficient which tends to follow a power-law function (due to the predominant influence of light scattering by non-algal particles). A very wide range of  $b$  values were encountered in the study areas (from less than 8 up to  $80 \text{ m}^{-1}$ ). Note also the steepest spectral variations of  $b$  in the almost freshwaters of the Río de la Plata as compared to the flatter ones observed in the Bay of Bourgneuf (Fig. 2(b)).

This may be related to the size distribution of suspended particles [4] and should be investigated further.

### 3.2 Absorption correction (ECO-BB)

Considering the exact design and dimensions of the ECO-BB sensor provided by WET Labs, our first results indicate that the instrument pathlength is actually shorter than indicated in the User's Guide, i.e., 0.01635 m instead of 0.0391 m. This has been communicated to and acknowledged by WET Labs which means that ECO-BB measurements are even less affected by absorption loss than previously stated. Therefore, Eq. (1) is re-written as:

$$\beta_{cor}(124^\circ, a_{nw} = 0) = \beta_{meas}(124^\circ, a_{nw}) \times \exp(0.01635 \times a_{nw}). \quad (6)$$

SimulO computations are then used to determine the actual angle of detected scattered photons when varying the particulate thus total scattering coefficient  $b$  of the water, i.e., increasing the SPM concentration. Results indicate that the mean backscattering angle of detected photons is actually slightly lower than stated by the manufacturer ( $121^\circ$  instead of  $124^\circ$ ) and tends to decrease (down to about  $115^\circ$ ) when  $c$  increases (Fig. 3(a)). This is logical as an increase of light attenuation along the instrument pathlength will favour shorter photon trajectories which correspond to smaller scattering angles. Now this decrease of the mean backscattering angle is balanced by the wide range of detected backscattering angles ( $\pm 16^\circ$ ) due to the large FOV of the sensor (Fig. 3(b)). It is important to note here that despite multi-scattering events (when  $b$  reaches values of  $10 \text{ m}^{-1}$  and up to  $50 \text{ m}^{-1}$ ), detected photons are those backscattered with an angle of about  $117^\circ$  ( $\pm 16^\circ$ ). This simply results from the shape of the VSF of marine particles which is highly peaked in the forward direction. Photons detected by the ECO-BB sensor in highly scattering waters have been scattered more than once several times in the forward direction but only once at an angle of about  $117^\circ$ . Consequently reliable light backscattering measurements can be performed in turbid scattering waters with such a device.

We finally applied the new correction (Eq. (6)) to simulated  $\beta$  measurements ( $\beta_{meas}$ ) to obtain  $\beta_{cor}$  values and examined the  $\beta_{cor}/\beta_{True}$  ratio ( $\beta_{True}$  being the actual values imposed in the simulations). Satisfactory results are obtained (Fig. 3(c)) showing measurement errors of only a few percent ( $\pm 4\%$ ), the true signal being typically slightly underestimated (probably due to uncorrected scattering effects). Once again there is no significant degradation of results when increasing the scattering coefficient of the water (here up to  $50 \text{ m}^{-1}$ ) which confirms that reliable and accurate particulate backscattering measurements can be made in turbid natural waters. This is due to small instrument pathlength and to the fact that the VSFs of marine particles are highly peaked in the forward direction.

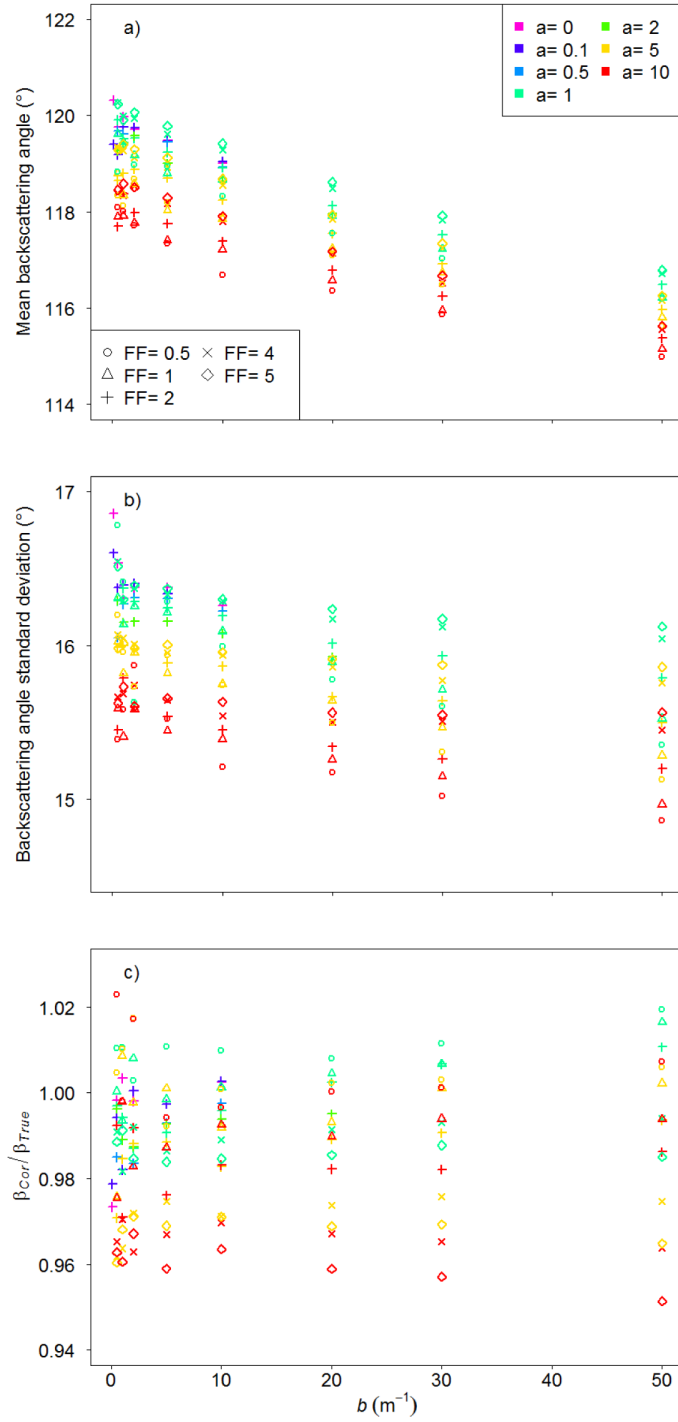


Fig. 3. Simulo results obtained for the ECO-BB sensor: (a) Variations of the mean backscattering angle of detected photons as a function of the water scattering coefficient,  $b$  in  $\text{m}^{-1}$ . (b) Standard deviation of the mean backscattering angle. (c) Ratio between the corrected and true  $\beta$  signals. Different colours and symbols, respectively, correspond to different values of absorption coefficients and Fournier-Forand (FF) particulate phase functions. Results from all simulated cases are shown.

### 3.3 Correction for absorption and scattering (Hydroscat)

The first question addressed concerning the Hydroscat sensors is whether  $K_{scat}$  in Eq. (3) is actually a constant value of 0.4 (as this has never been demonstrated that 40% of the photons scattered along their pathlength are systematically lost and not detected by the Hydroscat sensor). The second question addressed concerns the sensitivity of the  $K_{scat}$  coefficient to variations of the particulate backscattering ratio ( $b_{bp}/b_p$ , in %) which was observed to vary by up to a factor 6 in natural coastal waters [40–42]. SimulO computations are used to examine potential changes in  $K_{scat}$  when wide variations of  $b_{bp}/b_p$  (from 0.5 to 5%) are imposed. The sigma correction (Eqs. (2) and (3)) is used in reverse to derive, for each simulation, the  $K_{scat}$  value to obtain  $\beta_{cor} = \beta_{True}$ , i.e.:

$$K_{scat} = \frac{1}{b_p} \times \left( \frac{1}{k_{exp}} \times \ln\left(\frac{\beta_{True}}{\beta_{meas}}\right) - a_{nw} \right). \quad (7)$$

The resulting  $K_{scat}$  values were filtered to remove the cases of no interest (when light absorption was predominant over light scattering ( $a_{nw} > b_p$ ), when light attenuation along the instrument pathlength was too low ( $\beta_{meas}/\beta_{True} > 0.9$ ) and unexpected ( $K_{scat} < 0$ ). 45% and 55% of computed  $K_{scat}$  values, respectively for the HS-4 and HS-6, were kept for further analysis.

Striking results are obtained regarding the remaining values of the  $K_{scat}$  coefficient. Considering the virtual HS-4 sensor, the  $K_{scat}$  coefficient is actually found to vary from about 0 to 0.17, being much lower than the constant value of 0.4 set in the standard sigma correction (Fig. 4(a)). No correlation is found between  $K_{scat}$  and the imposed absorption, scattering or attenuation coefficients ( $a_{nw}$ ,  $b_p$  and  $c_{nw}$ , all excluding pure water contributions), no more than with the  $b_p/a_{nw}$  ratio (not shown).  $K_{scat}$  is actually observed to increase significantly (by a factor 5 at least) for increasing values of the  $b_{bp}/b_p$  ratio (Fig. 4). This appears to be logical, i.e., the more efficient are the particles at backscattering light, the more photons are lost along the instrument pathlength. Despite a clear increase of  $K_{scat}$  with increasing values of  $b_{bp}/b_p$ , no robust relationship can be established between the two variables. For a fixed  $b_{bp}/b_p$  ratio,  $K_{scat}$  is also influenced by variations of both  $a_{nw}$  and  $b_p$  (see the different colours and symbols points in Fig. 4(a)).

Now considering the virtual HS-6 sensor, slightly different results are obtained (Fig. 4(b)). The  $K_{scat}$  coefficient is higher than for the HS-4: it is observed to vary from about 0.05 to 0.22, being still much lower (by a factor 2 at least) than the constant value of 0.4 set in the standard sigma correction. Once again  $K_{scat}$  increases for increasing values of the  $b_{bp}/b_p$  ratio but no robust relationship can be established between the two variables. Note that some (at least 2) simulated cases show unexpected results with  $K_{scat}$  values higher than 0.4 (Fig. 4(b)). The formulation of the standard sigma correction (Eqs. (2) and (3)) with a constant  $k_{exp}$  value in Eq. (4) is even less valid when dealing with the large dimensions of the HS-6, i.e., with an instrument pathlength of about 0.15 m (Table 1). While the absorption and scattering coefficients of natural waters increase from almost 0 to 10 m<sup>-1</sup> and 50 m<sup>-1</sup>, respectively, the actual pathlength of detected photons certainly varies by several centimetres. In this case, a new formulation of the sigma correction method would be required, with a varying instrument pathlength (i.e., varying  $k_{exp}$  in Eq. (2)).

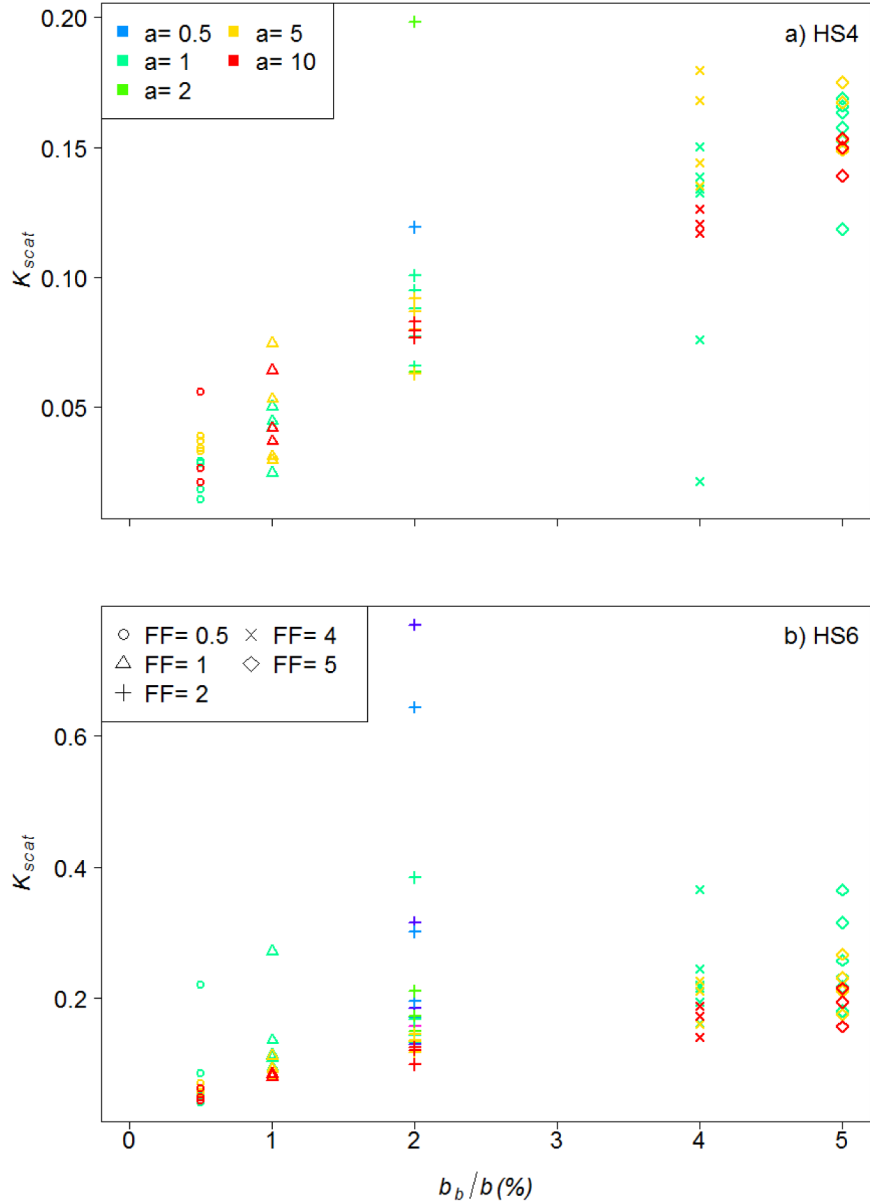


Fig. 4. Variations of the best-fitted  $K_{scat}$  coefficient as a function of the particulate backscattering ratio ( $b_{bp}/b_p$ ) for the HS-4 (a) and HS-6 (b) sensors. The particulate VSF is a Fournier-Forand (FF) with a  $b_{bp}/b_p$  ratio varying from 0.5 to 5%. Values for different absorption coefficients (total minus pure water contribution, in  $m^{-1}$ ) are shown in different colours. Cases corresponding to predominantly absorbing waters ( $a_{nw} > b_p$ ), low attenuation along instrument pathlength ( $\beta_{meas}/\beta_{True} > 0.9$ ) and unexpected cases ( $K_{scat} < 0$ ) were removed from the data set on this plot.

To summarize  $K_{scat}$  is clearly not a simple linear function of the absorption and scattering coefficients, and not only a function of the particulate backscattering ratio (Fig. 4). This is due to potentially complex trajectories of photons in multi-scattering regimes. In order to obtain better results we finally attempt to develop a new parametrization of  $K_{bb}$ . Based on Eqs. (3), (8) and (9), it may seem intuitive to express  $K_{bb}$  as a function of  $a_{nw}$  and  $b_{bp}$ , instead of  $a_{nw}$  and  $b_p$ . In this case we assume that photons lost along the instrument pathlength are mainly those

absorbed and scattered in the backward direction (plus probably a residual term corresponding to photons scattered in the forward direction but with an angle significantly different from the direction of propagation). This new parametrization is written as:

$$K_{bb} = a_{nw} + K_1 \times b_{bp} \quad (8)$$

where  $a_{nw}$  and  $b_{bp}$  in  $\text{m}^{-1}$  are respectively the absorption and backscattering coefficients excluding the contribution of pure water;  $K_1$  is an empirical constant value expected to be higher than 1.

Based on SimulO computations,  $K_{bb}$  is derived from Eq. (2) for each simulated case. Then in Eq. (10) where  $K_{bb}$  (computed),  $a_{nw}$  and  $b_{bp}$  (imposed) are known,  $K_1$  is obtained from the best linear fit between  $(K_{bb} - a_{nw})$  and  $b_{bp}$ . Results, respectively for the HS-4 and HS-6 sensors (Fig. 5), are:

$$\text{HS-4: } K_{bb} = a_{nw} + 3.30 \times b_{bp}, \quad R^2 = 0.96 \quad (9)$$

and:

$$\text{HS-6: } K_{bb} = a_{nw} + 4.34 \times b_{bp}, \quad R^2 = 0.92. \quad (10)$$

As expected, the  $K_1$  coefficient is higher than 1 as it corresponds to all photons scattered in the backward direction plus photons scattered in the forward direction with an angle significantly different from  $0^\circ$ . The  $K_1$  coefficients respectively obtained for the HS-4 and HS6 sensors are about three times and four times higher than 1. Analysis of SimulO computations results (not shown) indicate that it corresponds to all photons scattered with an angle higher than about  $10^\circ$  in a low scattering environment ( $b_p \leq 1 \text{ m}^{-1}$ ). In multi-scattering regimes, it is no longer possible to define an angle corresponding to the maximum scattering angle allowing detection. In average, over all our cases,  $K_1$  coefficients could be associated to a maximum scattering angle of  $43^\circ$  and  $37^\circ$ , respectively for the HS-4 and HS-6. Such angles may appear surprisingly high but one must keep in mind that most of the cases simulated correspond to complex photon trajectories when in multi-scattering regimes. These new parametrizations of  $K_{bb}$  for the HS-4 and HS-6 sensors appear as the most satisfactory ones and are selected for the rest of the study, notably for comparison with the standard sigma correction.

Now considering all our simulated cases (i.e., not only the cases considered in the  $K_{scat}$  and  $K_{bb}$  analyses), we look at the backscattering angle of photons detected by the HS-4: this angle is narrow ( $\pm 2^\circ$ ) and centred at  $142^\circ$  in the case of clear waters ( $a_{nw}$  and  $b_p$  close to  $0 \text{ m}^{-1}$ ) (Fig. 6(a-b)). As light scattering increases, this angle progressively decreases (down to about  $135^\circ$ ) and covers a much broader range as for the ECO-BB ( $\pm 15^\circ$ ) due to multi-scattering events. These first results are encouraging and suggest that reliable light backscattering measurements can be made with the HS-4, even in highly absorbing and/or scattering waters. This is confirmed when considering the ratio between the virtually measured then corrected (new correction using Eq. (9))  $\beta$  signal ( $\beta_{cor}$ ) and true (imposed) signal ( $\beta_{true}$ ). The results, also for all our simulated cases, are satisfactory as most of the values obtained vary from 0.95 to 1.05, i.e., errors in the range  $\pm 5\%$ , independently of the variations of  $b_p$  (Fig. 6(c)). This clearly indicates that our new correction method performs well even in highly scattering waters. Note that very similar results are obtained in the SWIR wavelength (1020 nm, black points in Fig. 6). Once applying a virtual calibration (see section 2.2) for this highly absorbing case (total absorption coefficient of  $30 \text{ m}^{-1}$ , due to light absorption by pure water), the effect on increasing light scattering on the mean backscattering angle and standard deviation, as well as the error associated to the  $\beta_{cor}$  signal are not different from those obtained in the virtual visible and NIR spectral regions. The new parametrisation of  $K_{bb}$  for the HS-4 (Eq. (9)) is therefore valid for a wide spectral domain (from the visible to the SWIR) and can be used to correct the data recorded with our prototype sensor.

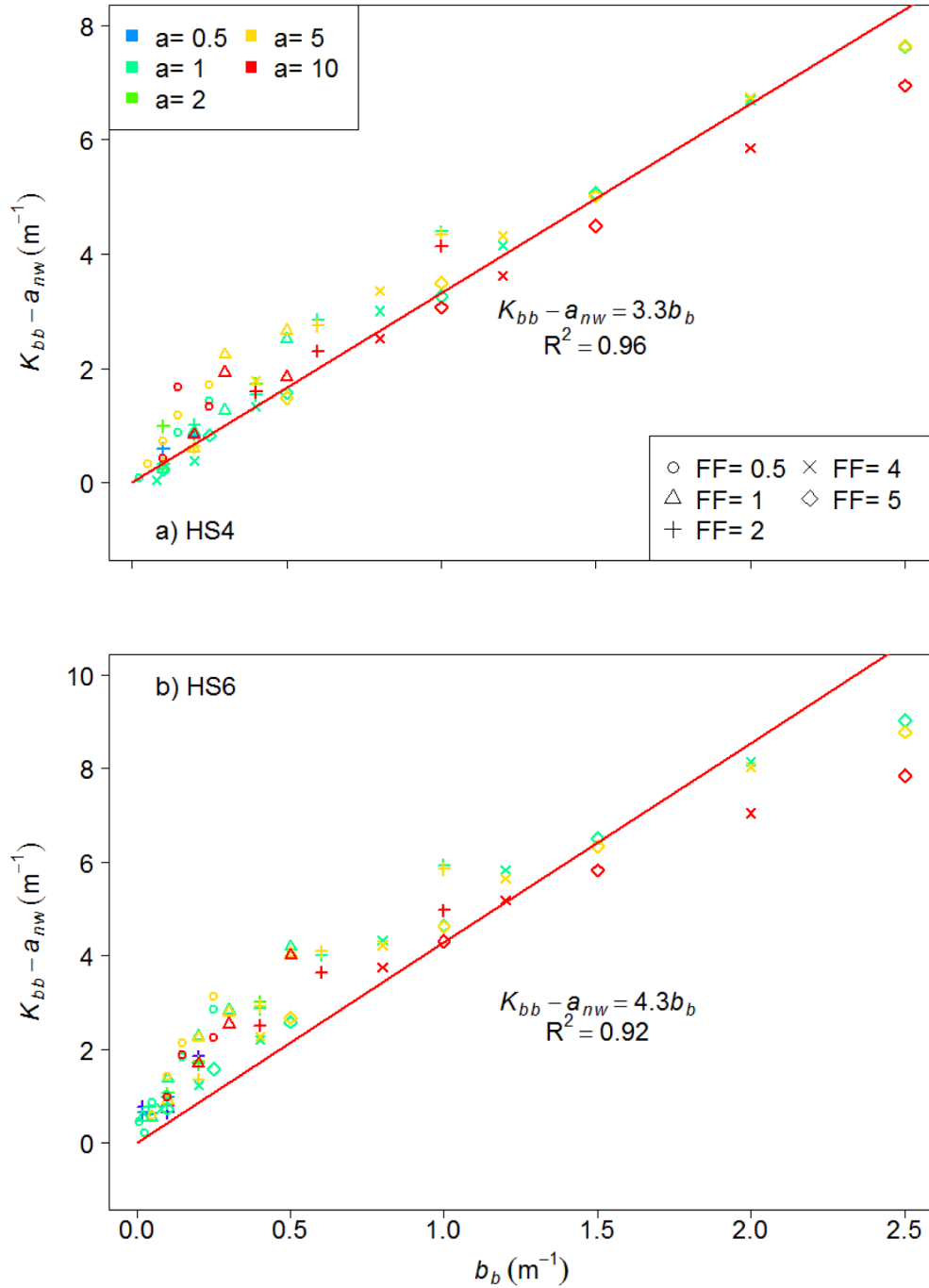


Fig. 5. Variations of  $(K_{bb} - a_{nw})$  as a function of  $b_b$ , based on SimulO computations, for the HS-4 (a) and HS-6 (b) sensors. Overplot of the best-fitted linear regressions with null intercept. Cases corresponding to predominantly absorbing waters ( $a_{nw} > b_p$ ), low attenuation along instrument pathlength ( $\beta_{meas}/\beta_{True} > 0.9$ ) and unexpected cases ( $K_{scat} < 0$ ) were removed from the data set on this plot.



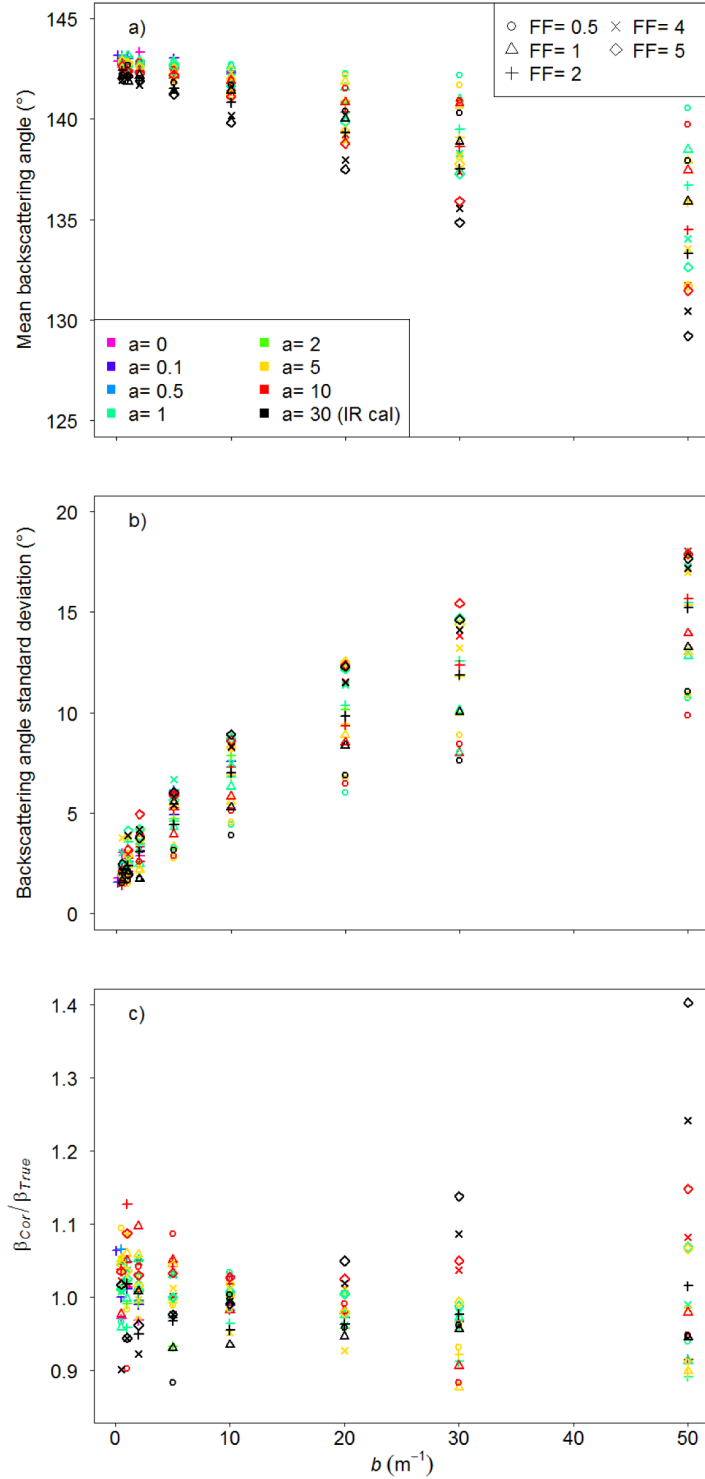


Fig. 6. Simulo results obtained for the HS-4 sensor. (a) Variations of the mean backscattering angle of detected photons as a function of the water scattering coefficient,  $b$  in  $\text{m}^{-1}$ . (b) Standard deviation of the mean backscattering angle as a function of  $b$ . (c) Ratio between the corrected (Eq. (11)) and true  $\beta$  signals. Results from all simulated cases are shown.

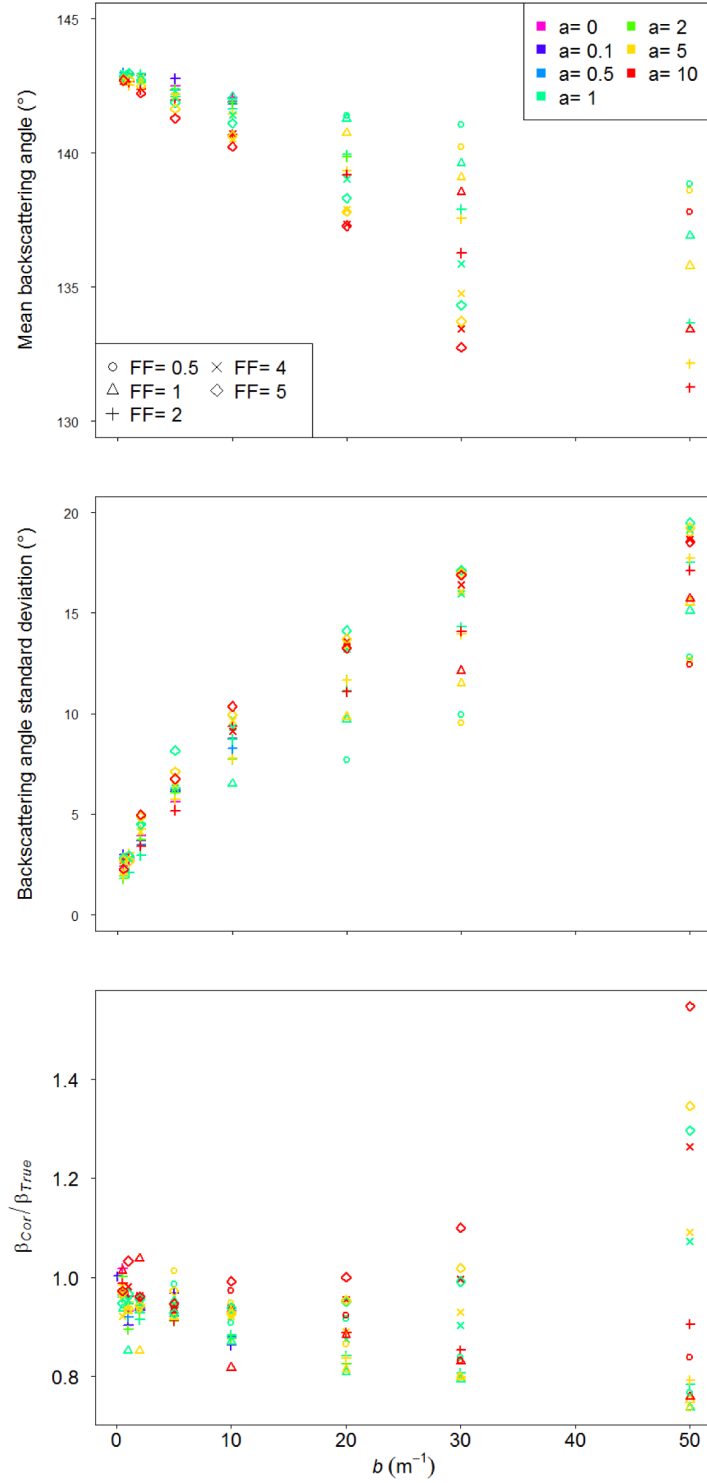


Fig. 7. Simulo results obtained for the HS-6 sensor. (a) Variations of the mean backscattering angle of detected photons as a function of the water scattering coefficient,  $b$  in  $\text{m}^{-1}$ . (b) Standard deviation of the mean backscattering angle as a function of  $b$ . (c) Ratio between the corrected (Eq. (12)) and true  $\beta$  signals. Results from all simulated cases are shown.

Similar results are obtained for the HS-6 but the effects of increasing light scattering on measurement errors are more pronounced. When  $b_p$  increases from 0 to 50  $\text{m}^{-1}$ , the mean backscattering angle decreases from 142° down to about 125° (Fig. 7(a)), but this does not necessarily represent an issue for estimating  $b_{bp}$ . As for the HS-4, the range of detected backscattering angles becomes progressively three times broader, increasing from about 3 to 15° (Fig. 7(b)), similar to the range covered by the ECO-BB. Results are less satisfactory regarding the error associated to  $\beta_{cor}$ : typically  $\pm 10\%$  when  $b_p$  is lower than 10  $\text{m}^{-1}$ ,  $\pm 20\%$  when  $b_p$  is higher than 10  $\text{m}^{-1}$ ; finally when  $b_p$  is as high as 50  $\text{m}^{-1}$ , the new correction leads to an overestimation of 5 to 50% of the  $\beta_{True}$  signal. In this case the dimensions of the HS-6 sensor are simply too large for measuring light backscattering due to complex trajectories of photons in multi-scattering regimes and significant variations of the nominal photon pathlength.

However, overall, results are satisfactory and both the ECO-BB and HS-4 sensors (when applying the new data correction method proposed in this study) should be able to perform reliable measurements in turbid waters to accurately estimate the particulate VSF. For such measurements in turbid waters the instrument pathlength is a key issue in the data correction: this pathlength should be as short as possible to minimize loss of photons due to scattering, which is the case with the ECO-BB sensor. This loss due to scattering must be taken into account and corrected for in the case of Hydroscat data. The new correction method developed in the present study (Eqs. (9) and (10)) assumes the loss of photons due to scattering along the instrument pathlength is, as a first approximation, a simple linear function of the particulate backscattering coefficient. Such a method, if proved to be valid based on real measurements, is convenient as it only requires measuring light absorption on top of Hydroscat data.

The next step is to test on field measurements the validity of our Monte Carlo simulation results. This test is made only considering Hydroscat measurements (HS-4) as to date only this sensor with its five adaptative gains has the capability to measure data without saturation in highly turbid scattering waters.

### 3.4 Assessment of standard and new sigma corrections (optical closure)

In order to assess the performance of the standard ( $K_{scat} = 0.4$ ) and new (Eq. (9) for the HS-4 sensor) sigma corrections, these two methods were applied to IOPs measured in the field in the Río de la Plata and Bay of Bourgneuf estuaries. When applying the new correction, a first approximation of  $K_{bb}$  was obtained at each wavelength using the measured  $\beta_{meas}$  values in Eq. (9):

$$K_{bb} = a_{nw} + 3.30 \times (2 \times \pi \times 1.08 \times (\beta_{meas} - \beta_w)), \quad (11)$$

where  $a_{nw}$  is the absorption coefficient measured using the AC-9 sensor, corrected for temperature, salinity and residual scattering effects (see section 2.3).

A first approximation of  $\beta_{cor}$  was obtained using Eq. (2), and used in Eq. (11) to obtain a second approximation of  $K_{bb}$  then of  $\beta_{cor}$  and so on. Using this iterative procedure, we systematically observed convergence of  $\beta_{cor}$  after a maximum of 5 iterations, while up to 10 iterations were allowed in our data processing code.

The resulting standard (s) and new (n) particulate backscattering coefficients, respectively noted  $b_{bp\_s}$  and  $b_{bp\_n}$ , were used as inputs in the Hydrolight radiative transfer code to compute the corresponding  $Rrs\_s$  and  $Rrs\_n$  synthetic values. Finally the obtained  $Rrs\_s$  and  $Rrs\_n$  values were compared to the measured  $Rrs$  (optical closure).

In the Río de la Plata, the  $Rrs$  signal measured with Trios sensors was first compared to  $Rrs$  measured using the ASD device in order to estimate the uncertainty associated to field data. Results showed a good agreement between the two independently measured signals: combining the 550, 700 and 850 nm, a linear relationship is observed ( $R^2 = 0.87$ ) with a slope of 1.02 and a negligible intercept. The mean relative difference between the two  $Rrs$  signals is 9.2% at 550 and 700 nm and 16.1% at 850 nm which confirms low measurement

uncertainties. An optical closure was therefore attempted using the  $Rrs$  values measured with the Trios (at 550, 700 and 850 nm) and ASD (at 1020 nm) as references to validate the computed  $Rrs_s$  and  $Rrs_n$  values. When combining the visible and NIR wavelengths, a linear relationship ( $R^2 = 0.82$ ) can be established between the measured  $Rrs$  (x axis) and computed  $Rrs_s$  (y axis) with a negligible intercept but the slope (2.25) is much higher than 1 (Fig. 8(a)). The standard sigma correction method dramatically overestimates the ‘true’  $Rrs$  signal. In contrast, a good agreement is observed between the measured  $Rrs$  and computed  $Rrs_n$  ( $R^2 = 0.86$ ): despite some scatter, a linear relationship is established with a negligible intercept and a slope (0.99) very close to 1 (Fig. 8(a)). At 1020 nm the correlation between measured and computed  $Rrs$  values significantly decreases due to a lower signal to noise ratio but similar results are obtained: linear relationships with negligible intercepts and a slope of 2.37 and 0.95, respectively, between the computed  $Rrs_s$  and  $Rrs_n$  (y axis) and the measured  $Rrs$  signal (x axis).

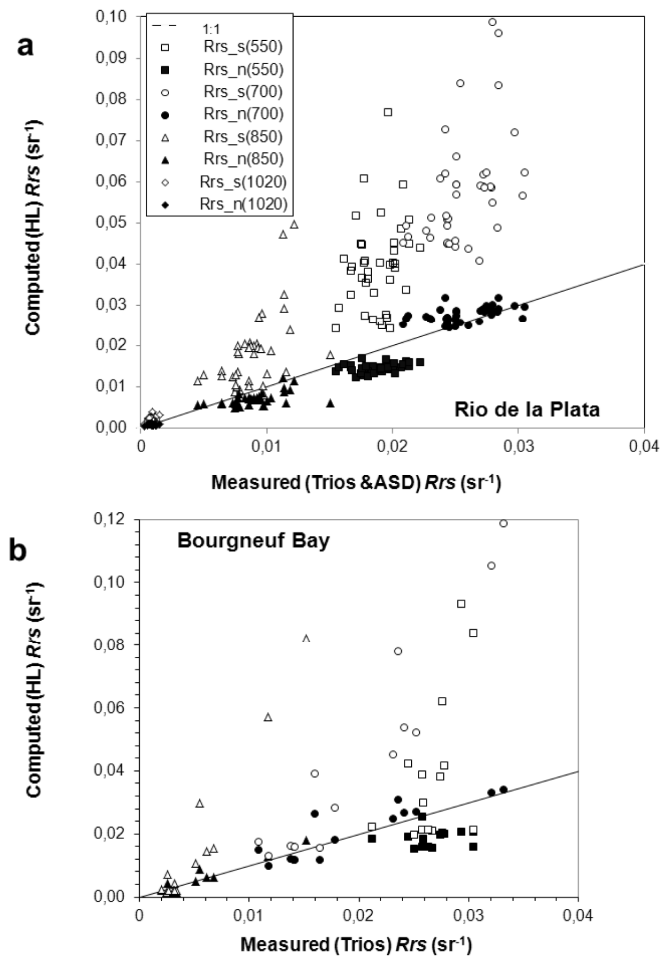


Fig. 8. (a) Optical closure obtained with the Río de la Plata data set. Plot of  $Rrs(550)$ ,  $Rrs(700)$ ,  $Rrs(850)$  and  $Rrs(1020)$  computed with Hydrolight using as inputs the  $b_{hp}$  values obtained from the standard sigma correction (white points) and new correction (black points) as a function of the  $Rrs$  values measured with the Trios (at 550, 700 and 850 nm) and ASD (at 1020 nm) sensors. (b) Optical closure obtained with the Bay of Bourgneuf data set. Plot of  $Rrs(550)$ ,  $Rrs(700)$ ,  $Rrs(850)$  and  $Rrs(1020)$  computed with Hydrolight using as inputs the  $b_{hp}$  values obtained from the standard sigma correction (white points) and new correction (black points) as a function of  $Rrs$  measured at the same wavelengths with the Trios sensors. The black lines show the 1:1 linear regression.

The Bourgneuf Bay data set tends to confirm these results. Combining the visible and NIR wavelengths, a rather poor linear relationship ( $R^2 = 0.48$ ) is observed between the measured  $Rrs$  (x axis) and computed  $Rrs\_s$  (y axis) with a negligible intercept and the slope close to 2 (1.98) (Fig. 8(b)). Actually the difference between  $Rrs$  and  $Rrs\_s$  increases with increasing  $Rrs$ , i.e., with increasing  $b_{bp}$ . The more light is scattered in the water the more  $Rrs\_s$  vs.  $Rrs$  departs from the 1:1 relationship. In contrast, once again, a linear relationship ( $R^2 = 0.74$ ) with negligible intercept and a slope close to 1 (0.86) is obtained between  $Rrs$  and  $Rrs\_n$ .

The new correction method applied to Hydrosat data allows a more accurate retrieval of the 'true'  $Rrs$  signal at 550, 700, 850 and 1020 nm while the standard sigma correction leads to an overestimation by a factor 2. This factor 2 difference between the computed  $Rrs\_s$  and  $Rrs\_n$  values results from the factor 2 to 4 difference between the  $b_{bp}$  values produced using the standard and new sigma corrections. The standard sigma correction clearly overestimates light attenuation along the photons pathlength due to particulate scattering, overcorrects for it and thus dramatically overestimates  $b_{bp}$  values in highly scattering waters.

### 3.5 Particulate backscattering ratio

Results presented in the previous section (optical closure) clearly suggest that the standard sigma correction (Eq. (3)) overcorrects Hydrosat data for light attenuation due to scattering, while the new correction method provides a correct estimation of measured multi-spectral  $Rrs$ . To confirm further this conclusion we examine the magnitude of the particulate backscattering ratio obtained when applying the two methods and compare it to values that have been reported in the literature for coastal waters [3, 40–42]. These values are expected to vary from 0.5 to 6%, around a mean value of 2%.

Values of the particulate backscattering ratio obtained when applying the standard sigma correction smoothly decrease with wavelength and could be modelled using a power-law function (Fig. 9(a)–9(b)). In terms of magnitude,  $b_{bp\_s}/b_p$  typically varies from 5 up to 15–20% in the Río de la Plata, from 3 up to 25–35% in the slightly more turbid waters of the Bourgneuf Bay. Such high values are definitely unexpected in the case of marine particles, which suggests once again that the sigma correction overcorrects Hydrosat data for light attenuation and provides dramatically overestimated  $b_{bp\_s}$  coefficients in highly scattering waters. Less pronounced spectral variations of the particulate backscattering ratio are obtained when the new correction method is applied to Hydrosat data (Fig. 9(c-d)):  $b_{bp\_s}/b_p$  spectra are almost flat in the Río de la Plata and only show a weak decrease with increasing wavelength in the Bourgneuf Bay, as already observed in U.S. coastal waters [40,41]. Moreover  $b_{bp\_s}/b_p$  values are in the expected range of magnitude in the two estuaries sampled, i.e., varying from 1.5 to 3.5% around a mean value close to 2%. Assuming the uncertainty associated to  $b_p$  obtained from AC-9 measurements is lower than 20% [12], this simple examination of the particulate backscattering ratio demonstrates the limits of the standard sigma correction in moderately to highly scattering waters; conversely it tends to validate the new correction method developed in this study (though the most straightforward validation remains the optical closure obtained with  $Rrs$  measurements).

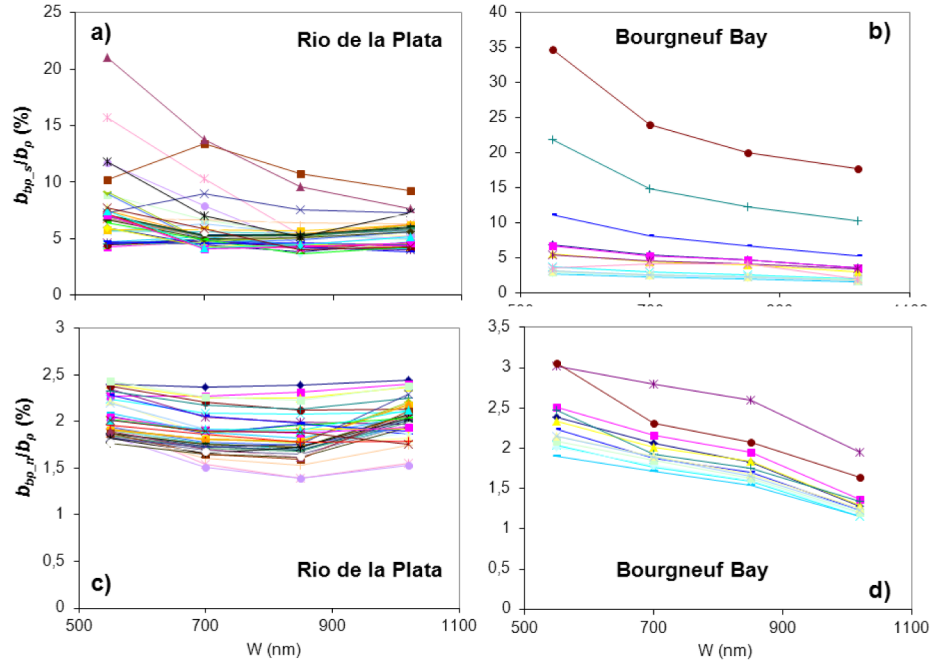


Fig. 9. Spectral variations of the particulate backscattering ratio, in %, measured in the Río de la Plata (left) and Bourgneuf Bay (right). The  $b_{bp,s}$  and  $b_{bp,n}$  particulate backscattering coefficients were respectively obtained by applying the standard (a-b) and new (c-d) correction methods to HS-4 data.

#### 4. Conclusions

A Monte Carlo code was used to reproduce the exact design of sensors made to measure light backscattering in natural waters, namely the WET Labs ECO-BB and HOBI Labs Hydroscat sensors. The IOPs of most natural waters were simulated by considering wide variations of the light absorption and scattering coefficients, and of the particulate VSF, and the validity of the data correction recommended by the manufacturers was assessed.

Results first showed that multi-scattering events are not really an issue since the VSF of marine particles is highly peaked in the forward direction. Results showed that the instrument pathlength is the key issue for measurements in turbid (highly scattering) waters. As long as this pathlength is short enough (e.g., less than 0.02 m for the ECO-BB), only loss of photons due to absorption should be taken into account and corrected for. We showed that the ECO-BB sensor is actually less sensitive to absorption effects than stated by the manufacturer (see Eqs. (1) and (6)). For longer pathlengths (e.g., about 0.10 and 0.15 m, respectively, for the HS-4 and HS-6 sensors), loss of photons due to scattering must be accounted for but the standard sigma correction recommended by the manufacturer was proved not to be valid. We proposed an improved version of this correction method for each sensor (see Eqs. (9) and (10), respectively, for the HS-4 and HS-6 sensors) which only requires light absorption measurements in addition to Hydroscat data. Applying this new correction method provides a reasonably accurate retrieval of  $\beta_p$  in all types of natural waters, except in the case of extremely high scattering coefficients where complex multi-scattering events make it very difficult to correct the measurements. The smaller HS-4 sensor should be preferably used in highly scattering waters (see Figs. 6 and 7). The ideal scattering sensor in the case of turbid waters would have the reduced dimensions of the ECO-BB (short instrument pathlength) and the adaptive gain of the Hydroscat to be sensitive in clear waters and not saturate in highly scattering waters (e.g., river plumes and estuaries).

We have compared the performance of the standard and improved (Eqs. (9) and (10)) versions of the sigma correction on Hydroscat measurements carried out in highly turbid estuarine waters. Conclusive results were obtained based on optical closure: applying the standard correction leads to dramatic overestimates of  $\beta_p$  then  $b_{bp}$  and  $Rrs$  while the new correction was proved to be valid and accurate enough to accurately measure in the field the particulate backscattering ratio and retrieve through radiative transfer computations the seawater reflectance signal measured independently (see Figs. 8 and 9).

### Acknowledgments

This study is part of the SeaSWIR project funded by the BELSPO agency and HIGHROC project funded by the European Community's Seventh Framework Programme (FP7/2007-2013) under grant agreement n° 606797. We gratefully thank D.R. Dana and R.A. Maffione (HOBI Labs Inc.) and M. Twardowski (WET Labs Inc.) for providing detailed information on the Hydroscat ECO-BB sensors design. Field experiments in the Río de la Plata and Bourgneuf Bay were respectively carried out as part of the SeaSWIR (P.I. E. Knaeps) and ANR-12-AGRO-0001 GIGASSAT (P.I. F. Pernet) research projects.